Recombinant Human Liver Medium-Chain Acyl-CoA Dehydrogenase: Purification, Characterization, and the Mechanism of Interactions with Functionally Diverse C_8-CoA Molecules†

Kevin L. Peterson, Eduard E. Sergienko, Yihe Wu, N. Ravi Kumar, Arnold W. Strauss,‡ Arland E. Oleson, Wallace W. Muhonen,§ John B. Shabb,§ and D. K. Srivastava*

Biochemistry Department, North Dakota State University, Fargo, North Dakota 58105

Received April 21, 1995; Revised Manuscript Received September 11, 1995®

ABSTRACT: We offer a large scale purification procedure for the recombinant human liver medium-chain acyl-CoA dehydrogenase (HMCAD). This procedure routinely yields 100−150 mg of homogeneous preparation of the enzyme from 80 L of the *Escherichia coli* host cells. A comparative investigation of kinetic properties of the human liver and pig kidney enzymes revealed that, except for a few minor differences, both of these enzymes are nearly identical. We undertook detailed kinetic and thermodynamic investigations for the interaction of HMCAD−FAD with three C_8-CoA molecules (viz., octanoyl-CoA, 2-octenoyl-CoA, and 2-octynoyl-CoA), which differ with respect to the extent of unsaturation at the α-β carbon centers; octanoyl-CoA and 2-octenoyl-CoA serve as the substrate and product of the enzyme, respectively, whereas 2-octynoyl-CoA is known to inactivate the enzyme. Our experimental results demonstrate that all three C_8-CoA molecules first interact with HMCAD−FAD to form corresponding Michaelis complexes, followed by two subsequent isomerization reactions. The latter accompany either subtle changes in the electronic structures of the individual components (in case of 2-octenoyl-CoA and 2-octynoyl-CoA ligands), or a near-complete reduction of the enzyme-bound flavin (in case of octanoyl-CoA). The rate and equilibrium constants intrinsic to the above microscopic steps exhibit marked similarity with different C_8-CoA molecules. However, the electronic structural changes accompanying the 2-octynoyl-CoA-dependent inactivation of the enzyme is 3−4 orders of magnitude slower than the above isomerization reactions. Hence, the octanoyl-CoA-dependent reductive half-reaction and the 2-octynoyl-CoA-dependent covalent modification of the enzyme occur during entirely different microscopic steps. Arguments are presented that the origin of the above difference lies in the protein conformation-dependent orientation of Glu-376 in the vicinity of the C_8-CoA binding site.

In a series of publications over the past four years, we have elaborated on several mechanistic aspects of the medium-chain acyl-CoA dehydrogenase (MCAD)-catalyzed[1] "dehydrogenase" and "oxidase" reactions (Johnson et al., 1992, 1993, 1994; Johnson & Srivastava, 1993; Kumar & Srivastava, 1994, 1995; Srivastava et al., 1995). Most of our previous studies have been performed utilizing the pig kidney enzyme and frequently utilizing indolepropionyl-CoA (IPCoA) and indoleacryloyl-CoA (IACoA) as the chromogenic substrate and product, respectively. The chromophoric potential of IACoA has allowed us to do the following: (1) probe the enzyme site environment (Johnson et al., 1992; Johnson & Srivastava, 1993); (2) determine the role of protein conformational changes during ligand binding and catalysis (Johnson et al., 1992, 1993); (3) detect a chromophoric intermediate (previously referred to as "X") during the course of the reductive half-reaction of the enzyme, which also exhibits properties of a charge-transfer complex (Johnson & Srivastava, 1993); (4) determine the molecular basis of the enzyme-catalyzed dehydrogenase and oxidase reactions (Johnson et al., 1994); (5) delineate the microscopic pathways of the reductive and oxidative half-reactions of the enzyme (Johnson et al., 1993); and (6) discover the role of the 3′,5′-ADP moiety of coenzyme-A thioester in catalysis (Srivastava et al., 1995). The insights gained from the above studies have been instrumental in deducing the kinetic mechanism of the enzyme utilizing octanoyl-CoA/2-octenoyl-CoA as the physiological substrate/product pair of the enzyme (Kumar & Srivastava, 1994, 1995). These studies have revealed a stringent role of protein conformational changes in influencing the electronic structures of FAD moiety and CoA-ligands, as well as in enzyme catalysis (Johnson et al., 1994; Kumar & Srivastava, 1994).

In recent years, medium-chain acyl-CoA dehydrogenase has received added attention due to its direct involvement in one of the major inborn errors of fatty acid metabolism (Roe & Coates, 1989). The deficiency of this enzyme in human patients (most frequently caused by replacement of

† This work was supported by grants from American Heart Association, Dakota Affiliate (to D.K.S.), National Science Foundation (MCB-9507292 to D.K.S.), and National Institutes of Health (AM-20407 to A.W.S.; GM-49849 to J.B.S.).

* To whom correspondence should be addressed.

‡ From Department of Pediatrics, Washington University School of Medicine, St. Louis, MO 63110.

§ From Department of Biochemistry and Molecular Biology, University of North Dakota School of Medicine, Grand Forks, ND 58202.

® Abstract published in *Advance ACS Abstracts,* November 1, 1995.

[1] Abbreviations: MCAD, medium-chain acyl-CoA dehydrogenase; IPCoA, 3-indolepropionyl coenzyme A; IACoA, *trans*-3-indoleacryloyl coenzyme A; FPCoA, furylpropionyl coenzyme A; FACoA, furylacryloyl coenzyme A; DPCoA, [4-(dimethylamino)phenyl]propionyl coenzyme A; DCCoA, 4-(dimethylamino)cinnamoyl coenzyme A; $FcPF_6$, ferrocenium hexafluorophosphate; FAD, flavin adenine dinucleotide; EDTA, ethylenediaminetetraacetic acid; Oca, octanoyl-CoA; Oce, 2-octenoyl-CoA; Ocy, 2-octynoyl-CoA; CT, charge-transfer complex; IPTG, isopropyl β-D-thiogalactopyranoside; CMC, critical micelle concentration; BSA, bovine serum albumin; SDS, sodium dodecyl sulfate; PAGE, polyacrylamide gel electrophoresis.

0006-2960/95/0434-14942$09.00/0

Lys by Glu at residue 304, the K304E mutation) is manifested in Reye syndrome-like symptoms, with episodes of hypoketotic hypoglycemia with coma, dicarboxylic acidemia, liver failure, and sudden infant death (Kelly et al., 1990; Matsubara et al., 1990; Yokota et al., 1990; Gregersen et al., 1991). To understand the molecular basis of loss of enzyme activity due to this mutation, recourse has been made to clone, express, and create site-directed mutants of human liver medium-chain acyl-CoA dehydrogenase (HMCAD; Kelly et al., 1987; Bross et al., 1990; Andresen et al., 1993; Brackett et al., 1994). A number of studies along these lines have led to several interesting suggestions related to protein folding, tetramer assembly, etc., of the wild-type and K304E mutant enzymes (Saijo et al., 1994; Yokota et al., 1992; Bross et al., 1993). Some of these studies have been illuminated by the availability of the X-ray crystallographic structure of pig liver MCAD, which shares extensive sequence homology with HMCAD (Kim et al., 1993; Kelly et al., 1987).

With the availability of the HMCAD-expression system (Bross et al., 1990; Brackett et al., 1994), we became interested in utilizing this recombinant enzyme toward our mechanistic goals. This was particularly prompted by the fact that, unlike the pig kidney enzyme, a variety of site-specific HMCAD mutants may be created, and such mutants will aid in deciphering the role(s) of specific amino acids in catalysis and the overall enzyme mechanism (Bross et al., 1990; Yokota et al., 1992). Towards this goal, we realized that the recombinant enzyme yield of the crude extract was considerably low, and the purification protocol routinely adopted for isolating the pig kidney enzyme was not appropriate for obtaining the homogeneous preparation of HMCAD. These led us to optimize the conditions for growing *Escherichia coli* containing the HMCAD-plasmid and develop a simple and efficient purification procedure for isolating HMCAD in bulk quantities (see below). Prior to this work, purification of the recombinant HMCAD has been reported by Bross et al. (1990, 1993).

In the case of pig kidney enzyme, we noted that the microscopic pathway for the MCAD−FAD + octanoyl-CoA (reductive half) reaction was similar to that observed for the MCAD−FAD + octenoyl-CoA interaction (Kumar & Srivastava, 1994). Both of these reactions were found to proceed via three consecutive (binding followed by two isomerization) steps, and the observed relaxation rate constants of the corresponding fast and slow steps for these reactions were nearly the same (eq 1).

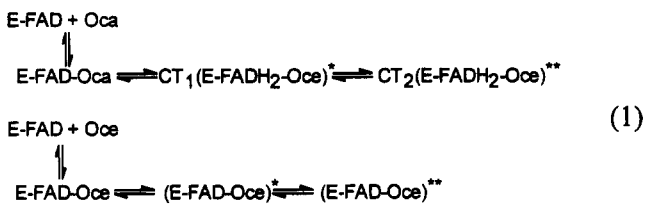

(1)

In eq 1, Oca and Oce represent octanoyl-CoA and 2-octenoyl-CoA, respectively. CT_1 and CT_2 are kinetically distinct forms of the first and second reduced enzyme−octenoyl-CoA charge-transfer complexes, respectively (Kumar & Srivastava, 1994).

The questions arose of whether or not the above features were common for the human liver enzyme and how similar or different was the microscopic pathway for the interaction of another C_8-CoA, 2-octynoyl-CoA, with HMCAD−FAD. This was particularly important since unlike octanoyl-CoA and 2-octenoyl-CoA (which function as substrate and product of the enzyme, respectively), 2-octynoyl had been known to inactivate the enzyme (Freund et al., 1985; Powell & Thorpe, 1988). In their detailed studies, Thorpe and his collaborators demonstrated that the 2-octynoyl-CoA-dependent inactivation of the pig kidney enzyme occurs due to a covalent modification of the γ-carboxyl group of an active site residue Glu-376 and argued that 2-octynoyl-CoA functions as a "mechanism-based" inactivator of the enzyme (Powell & Thorpe, 1988). Our interest in the 2-octynoyl-CoA-dependent inactivation of HMCAD emerged from two points of view: (1) What is the kinetic mechanism of inactivation of the enzyme by 2-octynoyl-CoA? To the best of our knowledge, no attempt has so far been made toward this goal. (2) Does the 2-octynoyl-CoA-dependent inactivation of the enzyme occur during an analogous microscopic step which is responsible for the octanoyl-CoA-dependent reductive half-reaction of the enzyme? As will be elaborated in the subsequent sections, the outcomes of these pursuits have thrown light on the similarities and differences between the microscopic pathways of interaction of the enzyme with structurally different α,β-unsaturated C_8-CoA ligands.

MATERIALS AND METHODS

Materials. Coenzyme A, octanoyl-CoA, acetoacetyl-CoA, EDTA, IPTG, ampicillin, chloramphenicol, and deoxyribonuclease I (Type II-S), and bovine serum albumin (BSA) were purchased from Sigma. 3-Indolepropionic acid, furylacrylic acid, 4-(dimethylamino)cinnamic acid, ferrocenium hexafluorophosphate, and 2-octynoic acid were purchased from Aldrich. Molecular weight standards for SDS−PAGE were purchased from Bio-Rad. The N-Z Amine media was purchased from Sheffield Products. Yeast extract and tryptone were purchased from Difco. All other reagents were of reagent grade.

Methods. 1. Expression, Growth of the Host Cells, and Extraction of Recombinant Human Liver Medium-Chain Acyl-CoA Dehydrogenase (HMCAD). The recombinant expression vector for HMCAD (pET11a-MCAD) has been prepared essentially as described by Brackett et al. (1994). The plasmid was transformed into *E. coli* BL21(DE3)pLysS host cells (Studier et al., 1990) by standard transformation methods (Sambrook et al., 1989).

The transformed cells were grown in M9ZB medium supplemented with 5 μg of riboflavin/mL, 50 μg of ampicillin/mL, and 25 μg of chloramphenicol/mL at 37 °C until the A_{600} was 0.5. Additional ampicillin (50 μg/mL) was added to the culture, and after 30 min, expression of HMCAD was induced by addition of IPTG to a final concentration of 0.5 mM. Incubation of the culture was continued for an additional 3 h. The cells were centrifuged at 5000g for 15 min. The pellet was washed with 50 mM Tris-HCl buffer (pH 8.0) and resuspended in the same buffer containing 2 mM EDTA. The suspension was stored frozen at −70 °C overnight. The cells were subjected to two freeze−thaw cycles and then treated with deoxyribonuclease I (1 μg/mL of suspension) to partially digest the chromosomal DNA and decrease the viscosity. The extract was centrifuged at 100 000g for 90 min, and the supernatant (crude extract) was stored frozen at −70 °C until the purification was started.

HMCAD activity was measured in 50 mM potassium phosphate buffer (pH 7.6) containing 0.3 mM EDTA at 25 °C, utilizing 150 μM indolepropionyl-CoA (IPCoA) and 250 μM ferrocenium hexafluorophosphate ($FcPF_6$) as described by Johnson et al. (1992). The enzyme activity is defined as the micromoles of IPCoA converted into IACoA per min under the above experimental conditions. The protein concentration was determined according to the Bradford method utilizing BSA as the standard protein (Bradford, 1976).

2. Purification of Recombinant HMCAD. The purification of the recombinant HMCAD (3.8 L of crude extract from 80 L of *E. coli* cell culture) was performed by adopting the following steps.

A. DEAE−Sephacel Column Chromatography: The crude extract was loaded onto a DEAE−Sephacel column (5 × 45 cm), previously equilibrated with 50 mM Tris-HCl containing 2 mM EDTA and 10% glycerol, pH 8.0 (4 °C). The column was washed with 6 column volumes of equilibrating buffer and then with 50 mM potassium phosphate buffer, pH 7.2, containing 2 mM EDTA and 10% glycerol until the A_{280} decreased to below 0.1. The HMCAD was eluted with a linear gradient of 0−250 mM NaCl in 50 mM phosphate buffer, pH 7.2, containing 2 mM EDTA and 10% glycerol. The fractions containing enzyme activity were pooled (total volume = 440 mL).

B. Hydroxyapatite column chromatography: The eluted fractions from the previous step (total volume = 440 mL) were supplemented with FAD (2−3-fold molar ratio of the MCAD−FAD sites) and then loaded onto a hydroxyapatite column (4 × 15 cm). The column was washed at 4 °C with 50 mM phosphate buffer, pH 7.2, containing 0.2 mM EDTA and 10% glycerol, until the A_{280} decreased to about 0.04. The HMCAD was eluted with a linear gradient of 50−500 mM of phosphate buffer, pH 7.2 containing 0.2 mM EDTA and 10% glycerol. The pooled fractions (total volume = 200 mL) were exhaustively dialyzed against 20 mM phosphate buffer, pH 7.6, containing 0.3 mM EDTA and 10% glycerol.

C. FPLC-TMAE column chromatography: The dialyzed enzyme was added with 2−3-fold molar excess (with respect to the MCAD−FAD sites) of FAD and divided into multiple 10 mL portions (containing about 45 mg of total protein). Each portion was loaded onto a Pharmacia FPLC−TMAE column (1 × 15 cm) that had been equilibrated with 20 mM phosphate buffer, pH 7.6, containing 0.3 mM EDTA and 10% glycerol. The column was washed with approximately two column volumes of equilibration buffer, and the HMCAD was eluted with a gradient of 0−1.0 M NaCl in 20 mM phosphate buffer, pH 7.6, containing 0.3 mM EDTA and 10% glycerol. The eluted enzyme fractions were pooled (total volume = 250 mL), concentrated in an Amicon 8200 ultrafiltration cell (with a PM-30 membrane), dialyzed against 50 mM phosphate buffer, pH 7.6, containing 0.3 mM EDTA, and stored frozen at −70 °C.

The protein concentration of the purified HMCAD was determined by the Bradford method (1976) and by measuring the absorbance at 446 nm. The extinction coefficient of HMCAD at 446 nm was taken as 15.4 mM^{-1} cm^{-1} (Thorpe et al., 1979). The protein concentration determined by these two methods differed by 7%−15%.

3. SDS−Gel Electrophoresis and Microsequencing of the Purified HMCAD. SDS−gel electrophoresis of the enzyme was performed according to Weber and Osborn (1969). The subunit molecular weight of the enzyme was determined using the Bio-Rad protein standard. A 20 μg portion of the purified enzyme was subjected to 24 cycles of sequencing on a Porton model 2090 gas phase protein sequencer at the Biopolymer Service Center of North Dakota State University.

4. Synthesis of Various CoA-Derivatives. Furylpropionic acid and [4-(dimethylamino)phenyl]propionic acid were prepared by catalytic reduction of their acrylic acids as described by Srivastava et al. (1995). The CoA-derivatives, 2-octynoyl-CoA, indolepropionyl-CoA (IPCoA), indoleacryloyl-CoA (IACoA), furylpropionyl-CoA (FPCoA), and [4-(dimethylamino)phenyl]propionyl-CoA (DPCoA), were prepared by the mixed anhydride procedure of Bernert and Sprecher (1977) and purified as described by Johnson et al. (1992). *trans*-2-Octenoyl-CoA was synthesized and purified according to Kumar and Srivastava (1994), and its extinction coefficient was taken as 20.4 mM^{-1} cm^{-1} (Kumar & Srivastava, 1994). The extinction coefficients of IPCoA, IACoA, FPCoA, DPCoA, and DCCoA were taken to be 18.2, 26.5, 16.0, 19.4, and 20.6 mM^{-1} cm^{-1} at 259, 367, 257, 250, and 400 nm, respectively (Srivastava et al., 1995). The extinction coefficients of FACoA and 2-octynoyl-CoA were taken to be 22.9 mM^{-1} cm^{-1} at 335 nm (McFarland et al., 1982) and 20.9 mM^{-1} cm^{-1} at 260 nm (Freund et al., 1985), respectively.

5. Steady-State and Transient Kinetic Experiments. The steady-state kinetic experiments for the enzyme-catalyzed dehydrogenase and oxidase reactions were performed on a Perkin-Elmer Lambda 3B spectrophotometer with a 1 or 10 cm path length cuvette. The standard buffer used for all steady-state experiments was 50 mM potassium phosphate containing 0.3 mM EDTA, pH 7.6, at 25 °C. The initial rates of the HMCAD-catalyzed reactions utilizing aliphatic acyl-CoA substrates were measured by following the reduction of ferrocenium hexafluorophosphate ($FcPF_6$) at 300 nm (ϵ_{300} = 4.3 mM^{-1} cm^{-1}; Lehman et al., 1990; Johnson et al., 1993). For chromogenic substrates, the initial rate measurements were made at the absorption maxima of their corresponding acryloyl-CoA products (see above).

The transient kinetic experiments were performed at 5 °C using an Applied Photophysics MV-14 sequential-mixing stopped-flow system (optical path length = 10 mm, dead time = 1.3−1.5 ms). The experimental results presented herein were obtained by configuring our stopped-flow device in a single-mixing mode. In this mode, the concentrations of reagents in syringes A and B were each diluted by 50%. The stopped-flow kinetic traces were analyzed by the data analysis package provided by Applied Photophysics.

6. Repetitive Rapid-Scanning Experiments. The time-dependent spectra during the course of interaction of HMCAD−FAD and 2-octynoyl-CoA were acquired with a Beckman 7400 diode array spectrophotometer with the help of a manual-mixing stopped-flow device (designed by Applied Photophysics). This device allows for a rapid mixing of reactants directly into a sealed spectrophotometric cuvette (path length = 10 mm), which fits nicely into a regular (10 mm × 10 mm) cuvette holder. An electronic circuit was designed to allow solution mixing to trigger the data acquisition by the diode array spectrophotometer. The dead-time of the instrument was determined by analyzing the kinetic profiles for the reaction of $K_2Cr_2O_7$ with KOH at 475 nm and was found to be approximately 100 ms. The

fastest time regime for spectral acquisition on this system was also 100 ms.

7. Determination of Dissociation Constants of HMCAD−FAD(H_2)−Octenoyl-CoA Complexes. The dissociation constant of the HMCAD−FAD−octenoyl-CoA complex was determined by spectrophotometric titration (at 442 nm) of a fixed concentration of HMCAD−FAD with increasing concentrations of 2-octenoyl-CoA. The data were analyzed by the classical quadratic equation for enzyme−ligand interactions (Schulz, 1994, p 23).

The equilibrium constant for the conversion of MCAD−$FADH_2$−octenoyl-CoA charge-transfer complex to MCAD−FAD + octanoyl-CoA was determined at 440 nm by acetoacetyl-CoA displacement method as described by Kumar and Srivastava (1995).

All the data analysis were performed by the nonlinear regression analysis software, Enzfitter (Biosoft).

8. Molecular Modeling. The atomic coordinates of pig liver MCAD in the absence (filename = 3MDD) and presence of C_8-CoA (filename = 3MDE) were downloaded from the Brookhaven Protein Data Bank and displayed on a Silicon Graphics Indigo XZ workstation. The protein structures were visualized by the aid of Insight II software (Biosym Technologies). The entire polypeptide backbone of the MCAD structure in the absence C_8-CoA ("apo") was superimposed with the identical residues of the MCAD structure in the presence of C_8-CoA ("holo") to a minimum rms deviation of 0.28 Å. Following this alignment, the distance measurements from various atoms were performed by Insight II.

RESULTS

Purification of Recombinant HMCAD. The transformation of pET11a-MCAD expression plasmid into *E. coli* BL21(DE3)pLysS host cells permitted a controlled induction of HMCAD in the presence of IPTG. When the above procedure was performed with host cells lacking pLysS, HMCAD was found to be induced even in the absence of IPTG, presumably due to some leakiness of the *lac* UV5 promotor upstream of the T7 RNA polymerase gene on the DE3 λ lysogen in the host (Studier et al., 1990). This basal level of T7 RNA polymerase is inhibited by T7 lysozyme encoded by the pLysS plasmid (Studier et al., 1990), and expression of the MCAD structural gene downstream of the T7 promotor is tightly regulated. The T7 lysozyme also helps in disruption of the host cells during the freeze−thaw cycles (see Materials and Methods). We observed that the presence of 10% glycerol during all the purification steps and the addition of FAD during the second and third column chromatographic steps improved the overall yield of the enzyme. The overall purification procedure was enhanced by the employment of two tandem column-chromatographic steps (without intervening dialysis), followed by FPLC−TMAE chromatography. These steps led to approximately 130-fold purification with 45% recovery of HMCAD (Table 1).

The purified HMCAD showed a single protein band of approximately 43 kDa (without any detectable contamination of other proteins) on SDS−polyacrylamide gel electrophoresis. This corresponds to the subunit molecular weight of the enzyme calculated from the nucleotide sequence analysis (Kelly et al., 1987). We subjected the purified HMCAD to protein microsequencing (figure not shown). Except for the first cycle (which was somewhat equivocal due to a minor amount of free amino acids contaminating the preparation), the sequence data from the following 23 cycles agreed exactly with the amino acid sequence predicted from the gene sequence of the mature human liver MCAD (Kelly et al., 1987).

Table 1: Summary of Purification of the Recombinant Human Liver Medium-Chain Acyl-CoA Dehydrogenase[a]

step	vol (mL)	tot. activity (units)	tot. protein (mg)	specific activity (units/mg)	fold purifn.	% yield
crude extract	3850	1294	37230	0.035	1.0	100
DEAE−Sephacel	440	1031	6675	0.15	4.3	79.7
hydroxyapatite	200	893	889	1.00	28.6	69.0
FPLC−TMAE	248	580	130	4.46	127.4	44.8

[a] From 80 L of *E. coli* culture.

Table 2: Comparative Steady-State Kinetic Parameters for the Human Liver and Pig Kidney MCAD-Catalyzed "Dehydrogenase" and "Oxidase" Reactions[a]

	human liver MCAD		pig kidney MCAD	
substrate	K_m (μM)	k_{cat} (s^{-1})	K_m (μM)	k_{cat} (s^{-1})
	Dehydrogenase Reaction			
C_4-CoA	450 ± 57.8	11.5 ± 0.5	264 ± 13.8	6.2 ± 0.1
C_6-CoA	6.8 ± 0.4	14.2 ± 0.3	3.6 ± 0.1	20.6 ± 0.2
C_8-CoA	3.0 ± 0.3	19.2 ± 0.3	2.3 ± 0.1	19.6 ± 0.2
C_{10}-CoA	2.9 ± 0.3	7.4 ± 0.3	0.94 ± 0.06	8.6 ± 0.1
FPCoA	14.4 ± 0.9	13.6 ± 0.3	14.4 ± 0.7	13.2 ± 0.2
IPCoA	8.7 ± 2.7	3.4 ± 0.03	10.3 ± 0.6	0.46 ± 0.01
DPCoA	42.6 ± 2.5	4.6 ± 0.07	61.0 ± 4.7	0.61 ± 0.01
	Oxidase Reaction			
IPCoA	nd	0.003	0.49 ± 0.04	0.016 ± 0.001

[a] Determined in 50 mM phosphate buffer, pH 7.6, containing 0.3 mM EDTA at 25 °C. K_m for acyl-CoAs and k_{cat} values for the dehydrogenase reaction were in the presence of 250−350 μM $FcPF_6$. These values for IPCoA-dependent oxidase reaction were measured in the presence of 240 μM buffer-dissolved oxygen.

Steady-State Kinetic Properties of Pig Kidney and Recombinant Human Liver MCADs. We determined the steady-state kinetic parameters of both pig kidney and recombinant human liver MCADs utilizing C_4 to C_{10} chain length (aliphatic) acyl-CoAs, as well as aromatic/heterocyclic ring-substituted propionyl-CoAs as chromogenic substrates. Table 2 summarizes the K_m and k_{cat} values for different acyl-CoA substrates (in the presence of saturating concentrations of ferrocenium hexafluorophosphate) during the pig kidney and human liver MCAD-catalyzed dehydrogenase reaction. For both these enzymes, there is a marked increase in the affinity of the substrate (decrease in K_m) upon increase in the chain length of acyl-CoAs from C_4 to C_6. After this, the increase in chain lengths of the acyl-CoA substrates (viz., from C_6 to C_8) shows small changes in the K_m and k_{cat} values for these enzymes. Due to their low critical micelle concentration (CMC) values (Zahler et al., 1968; our unpublished results), we did not utilize longer chain (>C_{10}) aliphatic acyl-CoA substrates in steady-state kinetic studies of these enzymes. Among chromogenic substrates, whereas the k_{cat}/K_m value for FPCoA is nearly identical for both the pig kidney and human liver enzymes, it is about one order of magnitude higher (with IPCoA and DPCoA as substrates) for the human liver enzyme than the pig kidney enzyme. Interestingly, the calculated k_{cat}/K_m ratios for IPCoA and DPCoA (involving the pig kidney enzyme) are similar to

that obtained with C_4-CoA. In this regard, it appears likely that the binding energy of the bulkier aromatic group of the acyl-CoA substrates is more efficiently utilized toward catalysis in the case of the human liver enzyme than the pig kidney enzyme (Jencks, 1987).

We observed that like the pig kidney MCAD (Srivastava et al., 1995), the human liver MCAD also catalyzes an "oxidase" reaction with a variety of acyl-CoA substrates. We investigated the steady-state kinetic parameters of the human liver MCAD-catalyzed oxidase reaction utilizing IPCoA as substrate. As shown in Table 2, the k_{cat} for the IPCoA-dependent oxidase reaction (in the presence of 240 μM buffer-dissolved oxygen) is approximately 5-fold lower for the human liver MCAD than that observed with pig kidney MCAD. Clearly, the human liver enzyme exhibits a reduced propensity to catalyze its physiologically undesirable oxidase reaction than the homologous enzyme from pig kidney.

Inactivation of HMCAD by 2-Octynoyl-CoA. In a preliminary manner, we ascertained that the 2-octynoyl-CoA-dependent inactivation of HMCAD was about 2 orders of magnitude slower than the turnover rates of the enzyme-catalyzed dehydrogenase reaction involving IPCoA as the substrate. This suggested to us that, in a reaction mixture of enzyme, substrate and the inactivator, the enzyme-catalyzed reaction would reach steady state before onset of the inactivation reaction. Under these conditions, the kinetic mechanism of the 2-octynoyl-CoA-dependent inactivation of the enzyme could be determined by analyzing the time-dependent reaction profiles of the enzyme-catalyzed reaction in the presence of varied concentrations of substrate and inactivator according to the theoretical model of Tsou (1988). While undertaking this approach, we realized (due to the reasons stated below) that the above reaction could best be studied by utilizing IPCoA rather than octanoyl-CoA as the enzyme substrate. (1) Due to a 6-fold higher extinction coefficient of IPCoA/IACoA than $FcPF_6$(oxidized)/$FcPF_6$-(reduced) pairs (Johnson et al., 1993), the enzyme-catalyzed reaction progress would yield significantly higher absorption changes with IPCoA than with octanoyl-CoA. Due to the nonchromogenic nature of octanoyl-CoA, the enzyme-catalyzed reaction progress was monitored by following the reduction of $FcPF_6$ at 300 nm. (2) In the presence of saturating concentrations of $FcPF_6$, the K_m for IPCoA is about 3-fold higher than the K_m for octanoyl-CoA (see Table 2). Hence, the reaction progress curves at subsaturating substrate concentrations would be more reliable with IPCoA than with octanoyl-CoA. (3) Since the K_m for $FcPF_6$ in the presence of saturating concentrations of IPCoA and octanoyl-CoA (with HMCAD) are 9.94 and 69 μM, respectively (our unpublished results), a lower concentration of $FcPF_6$ (giving lower background absorption at 367 nm) would be sufficient to achieve the saturated velocity in case of IPCoA substrate than with octanoyl-CoA substrate.

Figure 1A shows the time-dependent increase in absorption (at 367 nm) during the course of the HMCAD-catalyzed dehydrogenation of IPCoA (utilizing 200 μM $FcPF_6$) in the presence of increasing concentrations of 2-octynoyl-CoA. It is evident that the enzyme-catalyzed reaction shows a progressive decreasing trend with time (and finally attains a plateau) as the concentration of 2-octynoyl-CoA increases. As a consequence, the magnitude of the total absorption change (during the entire course of reaction) decreases with the increase in 2-octynoyl-CoA concentration (compare curves 1−6 of Figure 1A). The solid smooth lines are the best fit of the experimental data according to the single-exponential rate law (see Discussion).

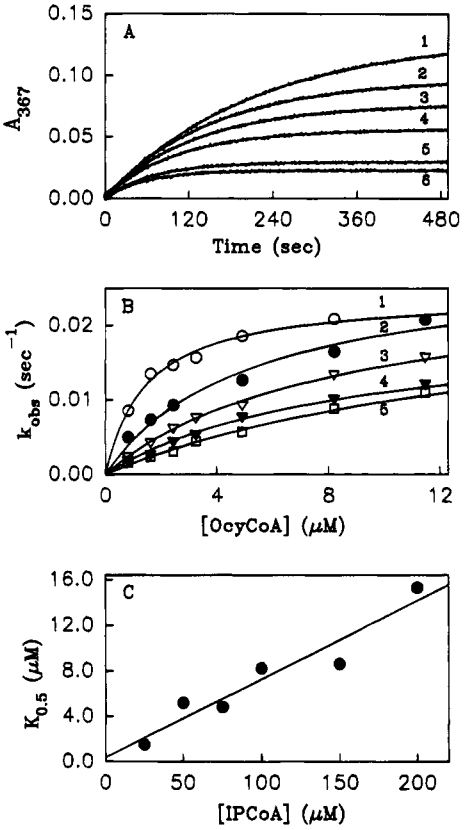

FIGURE 1: Recombinant human liver MCAD-catalyzed dehydrogenation of IPCoA in presence of 2-octynoyl-CoA in 50 mM phosphate buffer, pH 7.6, containing 0.3 mM EDTA at 25 °C. Panel A shows the time-dependent reaction progress in the presence of different concentrations of 2-octynoyl-CoA. $[E]_t = 7$ nM, [IPCoA] = 100 μM, $[FcPF_6] = 200$ μM; [2-octynoyl-CoA] for traces 1−6 were 1.6, 2.5, 3.3, 4.9, 8.2, and 11.5 μM, respectively. For clarity, several additional reaction traces are not included. The solid smooth lines are the best fit of the experimental data according to the single-exponential rate law. Panel B shows the dependence of single-exponential rate constants (k_{obs}), calculated from the traces of panel A, on 2-octynoyl-CoA concentrations. [IPCoA] for traces 1−5 were 25, 50, 100, 150, and 200 μM, respectively. The solid lines are the best fit of the experimental data for the hyperbolic dependence of k_{obs} on $[2\text{-octynoyl-CoA}]_t$ according to eq 6. The concentration of 2-octynoyl-CoA required to achieve the half-saturation ($K_{0.5}$) for the curves 1−5 are 1.5, 5.2, 8.2, 8.6, and 15.3 μM, respectively. The magnitude of k_{inact} at saturating concentrations of 2-octynoyl-CoA varies between 0.021 and 0.029 s^{-1}. Panel C shows the effect of [IPCoA] on $K_{0.5}$. The solid line is the best fit of the experimental data according to the linear dependence of $K_{0.5}$ on IPCoA according to eq 7. The slope (K_i/K_m) and the intercept (K_i) derived from this plot were 0.069 and 360 nM, respectively. From these values the K_m for IPCoA was calculated to be 5.2 μM.

We examined the effects of 2-octynoyl-CoA concentration on the observed rate constant (k_{obs}), derived from the data of Figure 1A. As shown in Figure 1B, the k_{obs} exhibits a hyperbolic dependence on the 2-octynoyl-CoA concentration at each concentration of IPCoA (curves 1−5). From this plot, the maximal rate constant for inactivation of the enzyme (k_{inact}) and the concentration of 2-octynoyl-CoA required to achieve half of the total changes in the rate constant ($K_{0.5}$) can be obtained. As will be discussed subsequently, the hyperbolic dependence of k_{obs} on 2-octynoyl-CoA concentration is suggestive of the fact that the inactivation proceeds

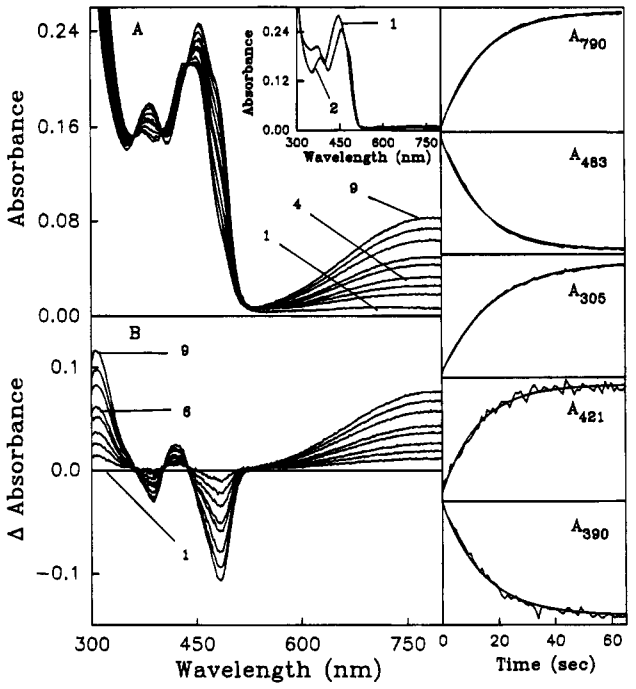

FIGURE 2: Repetitive rapid-scanning spectra for the reaction of HMCAD−FAD and 2-octynoyl-CoA. Panel A shows the time-dependent spectral changes for the reaction of 20 μM HMCAD−FAD with 287 μM 2-octynoyl-CoA (concentrations after mixing). The time sequences for the traces in panel A were (in seconds): (1) 0.1, (2) 3.0, (3) 5.0, (4) 7.0, (5) 10.0, (6) 12.0, (7) 18.0, (8) 25.0, and (9) 40. For clarity, the spectral traces at other time regimes are not shown. The inset of panel A shows the zero-time spectrum (generated by adding the spectra of the enzyme and 2-octynoyl-CoA without reaction; trace 1) and the first spectrum (obtained within 100 ms; trace 2). Panel B shows the difference spectra, which were derived after subtracting the first spectrum (trace 1) from the spectra at different times (traces 2−9). The panels on the right side represent the time slices of the spectra (of panel A) at different wavelengths. The single-exponential rate constants derived from the best fit of the experimental data (solid smooth lines) at different wavelengths are as follows: for 790 nm, 0.07 ± 0.001 s^{-1}; for 483 nm, 0.073 ± 0.001 s^{-1}; for 305 nm, 0.056 ± 0.001 s^{-1}; for 421 nm, 0.078 ± 0.003 s^{-1}; and for 390 nm, 0.071 ± 0.002 s^{-1}.

following the formation of the enzyme−octynoyl-CoA complex.

We further examined the effects 2-octynoyl-CoA on k_{obs} at different initial concentrations of the substrate, IPCoA. The curves 1−5 of Figure 1B are the best fit of the experimental data for the hyperbolic dependence of k_{obs} on 2-octynoyl-CoA (see above and Discussion). Note that as the initial concentration of IPCoA increases (curves 1−5), the hyperbolic curves attain asymptotes at higher concentrations of 2-octynoyl-CoA. From these data, we ascertained the magnitudes of $K_{0.5}$ and k_{inact} as functions of the initial concentrations of IPCoA. Of these parameters, whereas k_{inact} remains essentially invariant, $K_{0.5}$ exhibits a linear dependence on IPCoA concentration (Figure 1C). The latter profile is suggestive of the fact that IPCoA and 2-octynoyl-CoA interact competitively at the active site of the enzyme (see Discussion).

Spectral and Kinetic Profiles for HMCAD−FAD and 2-Octynoyl-CoA Interaction. Figure 2 shows the time-dependent spectral changes (obtained via our newly configured repetitive rapid-scanning device; see Materials and Methods) upon mixing 40 μM HMCAD−FAD and 574 μM 2-octynoyl-CoA (the concentrations of these species after mixing are 20 and 287 μM, respectively). The inset of Figure 2A compares the zero-time spectrum (i.e., the sum of the spectra of MCAD−FAD and 2-octynoyl-CoA without reaction) and the first spectrum (about 100 ms after mixing of the above reactants). These spectral data are consistent with the isosbestic points at 387, 398, 472, and 518 nm, and the maximal absorption changes at 353, 420, and 490 nm. The spectral data of Figure 2 reveal that following the rapid spectral change (see above), the subsequent spectral changes are considerably slower. Figure 2B shows the difference spectra, i.e., the spectra at different time regimes minus the first spectrum. These spectral data are consistent with the isosbestic points at 362, 405, 438, and 528 nm, and the maximal absorption changes at 305, 390, 421, 483, and 790 nm. Clearly, the isosbestic points and the maximal absorptions are different during the fast (inset of Figure 2A) and slow (Figure 2B) time regimes for the HMCAD−FAD + 2-octynoyl-CoA reaction. These differences suggest the events during the fast spectral changes are different than those during the slow spectral changes (see below and Discussion). We did not investigate the reaction phase (half-life = 12 min), which has been reported to originate due to hydrolysis of 2-octynoyl-CoA thioester (Freund et al., 1985).

Given that the overall spectral changes shown in Figure 2 occur in two different time regimes, the kinetic profiles of these changes were ascertained separately. The time-dependent slow spectral changes (right hand side panels of Figure 2) were extracted from the repetitive rapid-scanning data of Figure 2A by taking absorption slices at different wavelengths. The solid smooth lines of these panels are the best fit of the experimental data according to the single-exponential rate law, with rate constants varying from 0.056 to 0.079 s^{-1}. These values are 2−3-fold higher than the k_{inact} (0.021−0.029 s^{-1}) derived from the data of Figure 1B. We also determined the maximal rate of inactivation of HMCAD by measuring the time-dependent loss of the enzyme activity (under pseudo-first-order conditions; $[E]_t \ll [2\text{-octynoyl-CoA}]_t$) in an incubation mixture containing HMCAD and 2-octynoyl-CoA [such as described by Johnson and Srivastava (1991)] and determined its magnitude to be 0.060 ± 0.003 s^{-1} (data not shown). These results suggest that the slow spectral changes of Figure 2 are due to the 2-octynoyl-CoA-dependent inactivation of the enzyme. This conclusion is somewhat contrary to that of Freund et al. (1985), who claim that the above spectral changes are faster than the inactivation of the pig kidney enzyme. We offer no explanation for this discrepancy.

Since the rapid spectral change upon interaction of enzyme with 2-octynoyl-CoA is completed within 100 ms (see the inset Figure 2A), the kinetics of this fast reaction were investigated (at 5 °C) by the single-wavelength stopped-flow technique. Figure 3 shows the time-dependent absorption changes for the reaction of 15 μM HMCAD−FAD and 287 μM 2-octynoyl-CoA (concentrations after mixing) at 420 (Figure 3A) and 353 nm (Figure 3B). At both of these wavelengths, the reaction traces are best fitted by a biphasic rate equation. When attempts were made to fit these traces by a single-exponential rate equation, systematic deviation of residuals were observed (data not shown). The rate constants for the fast and slow phases at 420 were found to be 812 ± 18.4 and 34.1 ± 5.3 s^{-1}, respectively, and those at 353 nm were found to be 1040 ± 34.3 and 33.5 ± 3.2 s^{-1}, respectively. The amplitudes for the fast and slow

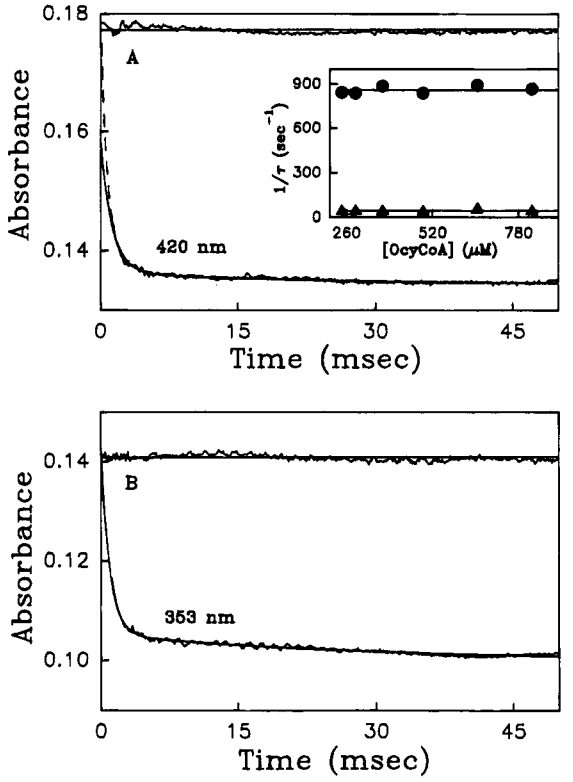

FIGURE 3: Single-wavelength stopped-flow traces for the reaction of HMCAD−FAD and 2-octynoyl-CoA at 5 °C. The concentrations of HMCAD−FAD and 2-octynoyl-CoA after mixing were 15 and 287 μM for the reaction trace at both 420 nm (Figure 3A) and 353 nm (Figure 3B). Other reaction conditions were the same as Figure 1. In each panel the "reaction" (biphasic) and "control" (horizontal) traces were obtained under identical experimental conditions. The horizontal control traces represent the sum of absorptions of HMCAD−FAD and 2-octynoyl-CoA when mixed against buffer via the stopped-flow syringes. The solid smooth lines are the best fit of the experimental data (for the reaction traces) according to the two-exponential rate equation. The fast and slow relaxation rate constants at 420 nm (Figure 3A) and 353 nm (Figure 3B) obtained from the best fits were found to be 812 ± 18.4 and 34.1 ± 5.3 s^{-1} and 1040 ± 34.3 and 33.5 ± 3.2 s^{-1}, respectively. The dotted line of Figure 3A is the best fit of the experimental data (according to a double-exponential rate equation) when the fast rate constant is fixed at 1240 s^{-1}. The inset of Figure 3A shows the 2-octynoyl-CoA concentration-dependent (after mixing concentrations) fast (filled circles) and slow (filled triangles) relaxation rate constants ($1/\tau$) measured at 420 nm.

phases at 420 and 353 nm were as follows: $A_{fast}(420)$ = 0.023, $A_{slow}(420)$ = 0.0021, $A_{fast}(353)$ = 0.038, $A_{slow}(353)$ = 0.0055. It should be pointed out that due to smaller amplitudes of the slow phases (vis-à-vis those of the faster phases) at these wavelengths, the kinetic traces of Figure 3 do not exhibit pronounced biphasicity, particularly upon visual inspection. Our assessment of these reaction traces being biphasic rather than monophasic is based on the best fitting results by the corresponding rate equations.

To account for the magnitude of absorption changes at 420 and 353 nm prior to the observed relaxation phases (see Figure 3), we compared the zero-time absorptions of the biphasic reaction traces (obtained by their extrapolation to zero-time) with the sum of absorptions of HMCAD−FAD and 2-octynoyl-CoA (without reaction). The latter was obtained by mixing the individual components against buffer via the stopped-flow syringes, followed by summations of the resultant time-dependent traces (see the horizontal traces of Figure 3A,B). Upon comparing these "control" (horizontal) traces with the zero-time absorption values of the complementary (biphasic) reaction traces, it appears that at 353 nm there is no evidence of absorption changes prior to the observed relaxation phases (within the dead-time of our stopped-flow; see Figure 3B). This does not appear to be the case for the absorption traces at 420 nm. At the latter wavelength, the horizontal trace intersects on the *Y*-axis at about 0.02 absorption unit higher than the extrapolated zero-time absorption value of the reaction trace (see Figure 3A), suggesting that some absorption changes may occur prior to the observed relaxation phases.

While contemplating the origin of the above discrepancy, we realized the extrapolated zero-time absorption values of the reaction traces may not be accurate. This is because their magnitudes are primarily determined by the rate constants that are greater than 800 s^{-1}, and such values are difficult to accurately determine with our stopped-flow device. For a reaction proceeding with a rate constant of 800 s^{-1}, about 67% of the reaction is completed within the 1.4 ms of dead-time of our stopped flow, and thus the evaluation of the overall rate constant is based on the analysis of only 33% of the remaining reaction phase. This may result into an inaccurate estimate of the zero-time absorption value of the reaction trace at 420 nm and may lead to the above discrepancy. This is attested by the fact that when the biphasic reaction trace at 420 nm is analyzed by fixing the fast rate constant at 1240 s^{-1} (dotted lines of Figure 3A), the extrapolated zero-time absorption value matches with that of the control (horizontal) trace. In light of these arguments, we believe that no absorption changes occur prior to the observed relaxation phases at 420 and 353 nm during the transient course of reaction between HMCAD−FAD and 2-octynoyl-CoA.

Comparison of the reaction traces of Figures 2 (right panels) and 3 reveals that the rate constants derived from the data of Figure 3 are at least 3−4 orders of magnitude faster than the rate constant for the slow spectral changes (Figure 2, right panels) during the course of inactivation of the enzyme. Hence, the sequence of events during the biphasic reaction profiles of Figure 3 must occur prior to the inactivation of the enzyme.

To probe the physical basis of the above phenomena, we investigated the 2-octynoyl-CoA concentration dependence of the fast and slow relaxation rate constants of Figure 3A at 420 nm, under the pseudo-first-order condition ($[E]_t \ll [2\text{-octynoyl-CoA}]_t$). As shown in the inset of Figure 3A, the observed relaxation rate constants show no apparent dependence on the 2-octynoyl-CoA concentration between 246 and 820 μM. This suggests that the absorption changes at 420 nm occur after the formation of the enzyme−octynoyl-CoA collision/Michaelis complex. Hence, the rapid absorption change shown in the Figure 2A inset is due to two subsequent isomerizations of the enzyme−octynoyl-CoA Michaelis complex (see Discussion).

Kinetic Profiles for the Interactions of Octanoyl-CoA and 2-Octenoyl-CoA with HMCAD−FAD. We performed the transient kinetic experiments for the interactions of octanoyl-CoA and 2-octenoyl-CoA with HMCAD−FAD (at 5 °C) by monitoring the absorbance changes at 450 and 545 nm for octanoyl-CoA and at 297 and 442 nm for 2-octenoyl-CoA, respectively (Figure 4A,B). All of these kinetic traces are best fitted by the biphasic rate equation. The observed fast ($1/\tau_{fast}$) and slow ($1/\tau_{slow}$) relaxation rate constants as well

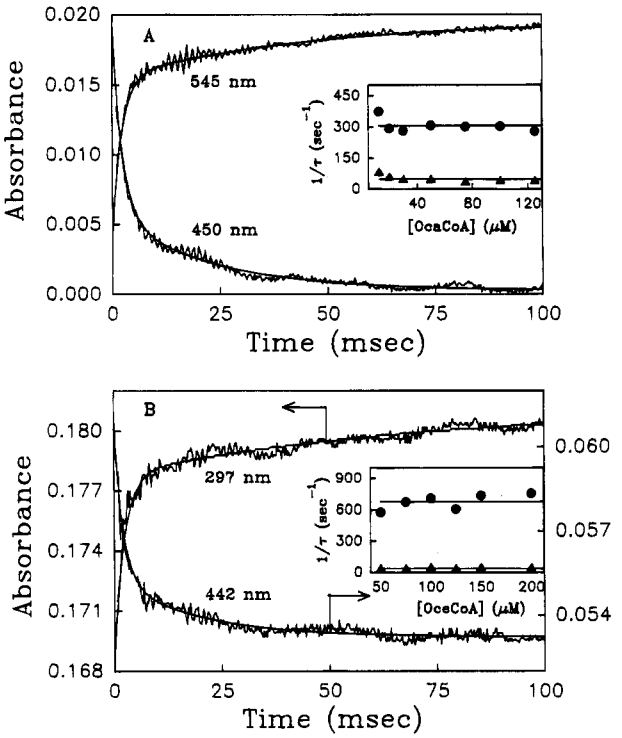

FIGURE 4: Transient kinetics for the octanoyl-CoA-dependent reductive half-reaction (panel A) and the HMCAD−FAD + 2-octenoyl-CoA interaction (panel B) at 5 °C. Other conditions were the same as in Figure 1. Panel A shows the single-wavelength stopped-flow traces at 450 nm (the oxidized flavin region) and at 545 nm (the charge-transfer complex region) for the HMCAD−FAD + octanoyl-CoA reaction. The concentrations of HMCAD−FAD and octanoyl-CoA after mixing were 1.25 and 50 μM for the trace at 450 nm and 5 and 50 μM for the trace at 545 nm, respectively. Solid smooth lines are the best fit of the experimental data according to the two-exponential rate equation. The fast and slow relaxation rate constants derived from these fits were 435 ± 16.9 and 44.2 ± 1.8 s^{-1} at 450 nm and 447 ± 18.8 and 22.5 ± 1.6 s^{-1} at 545 nm, respectively. The inset shows the octanoyl-CoA (after mixing) concentration-dependent fast (filled circles) and slow (filled triangles) relaxation rate constants ($1/\tau$) at 450 nm. Panel B shows the single-wavelength stopped-flow traces for the HMCAD−FAD + 2-octenoyl-CoA reaction at 297 nm (increasing phase) and 442 nm (decreasing phase). The concentrations of HMCAD−FAD and 2-octenoyl-CoA after mixing were 5 and 125 μM for the reaction trace at 297 and 442 nm. The fast and slow relaxation rate constants obtained from the best fit of the experimental data were 429 ± 19.1 and 14.4 ± 1.4 s^{-1} at 297 nm and 482 ± 52.9 and 53.4 ± 6.4 s^{-1} at 442 nm, respectively. The inset shows the 2-octenoyl-CoA (after mixing) concentration dependence of the fast (filled circles) and slow (filled triangles) relaxation rate constants ($1/\tau$) for the reaction measured at 297 nm.

as their corresponding amplitudes (A_{fast} and A_{slow}) for the data of Figure 4 are as follows: 450 nm, $1/\tau_{fast}$ = 435 ± 16.9, $1/\tau_{slow}$ = 44.2 ± 1.8 s^{-1}, A_{fast} = 0.014, A_{slow} = 0.0054; 545 nm, $1/\tau_{fast}$ = 447 ± 18.8, $1/\tau_{slow}$ = 22.5 ± 1.6 s^{-1}, A_{fast} = 0.012, A_{slow} = 0.004; 297 nm, $1/\tau_{fast}$ = 429 ± 19.1, $1/\tau_{slow}$ = 14.4 ± 1.4 s^{-1}, A_{fast} = 0.010, A_{slow} = 0.0034, 442 nm, $1/\tau_{fast}$ = 482 ± 52.9, $1/\tau_{slow}$ = 53.4 ± 6.4 s^{-1}, A_{fast} = 0.0056, A_{slow} = 0.0034.

To account for the magnitude of absorption changes prior to the observed relaxation phases of Figures 4A,B, we compared the zero-time absorptions of these traces (obtained by extrapolation of the biphasic fitted lines to zero-time) with the sum of absorptions of individual components, as performed in case of HMCAD−FAD + 2-octynoyl-CoA reaction (see Figure 3A,B and related texts). Such comparisons, for all the reaction traces of Figure 4A,B, revealed that the absorption changes prior to the observed relaxation phases are negligible for the HMCAD−FAD + octanoyl-CoA and HMCAD−FAD + octenoyl-CoA reactions (data not shown).

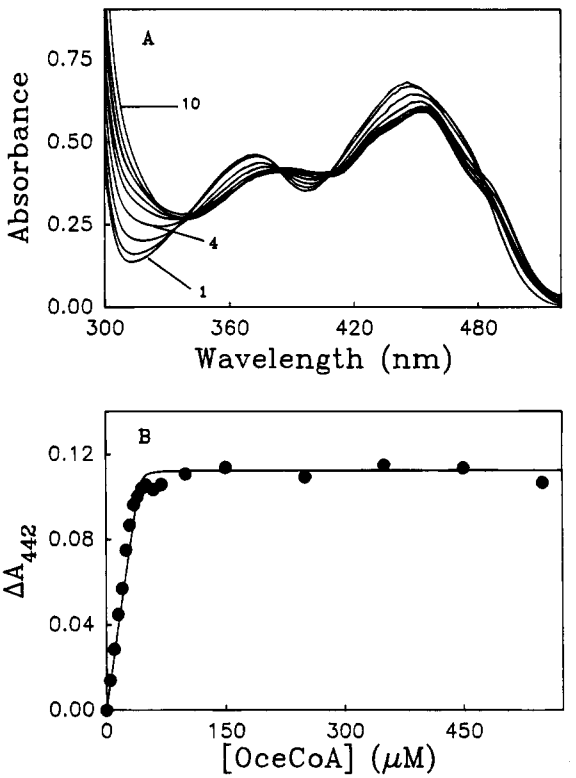

FIGURE 5: Titration of HMCAD−FAD with 2-octenoyl-CoA. Panel A shows the spectral changes during the course of titration of a fixed concentration of HMCAD−FAD (45 μM, spectrum 1) with increasing concentrations of 2-octenoyl-CoA (spectra 2−10). Panel B shows a plot of the absorption changes at 442 nm against the total concentration of 2-octenoyl-CoA. The solid line is the best fit of the experimental data for a dissociation constant of 153 nM.

We further investigated the octanoyl-CoA and 2-octenoyl-CoA concentration dependent (under pseudo-first-order conditions) fast and slow relaxation rate constants for the reactions of Figure 4A,B. As observed for the interaction of 2-octynoyl-CoA with HMCAD−FAD (Figure 3), both fast and slow relaxation rate constants remain invariant upon increasing the concentrations (after-mixing) of octanoyl-CoA from 12.5 to 125 μM (inset Figure 4A) and of 2-octenoyl-CoA from 50 to 200 μM (inset Figure 4B). A cumulative account of these results suggests that irrespective of the reaction type (viz., chemical transformation versus electronic structural changes), all the C_8-CoAs employed herein (viz., octanoyl-CoA, 2-octenoyl-CoA, and 2-octynoyl-CoA) initially interact with the enzyme site and form Michaelis complexes before undergoing two isomerization reactions, with similar magnitudes of their relaxation rate constants.

It should be pointed out that the fast relaxation rate constants obtained from the data of Figure 4A,B are about 2−3-fold lower than those observed during the course of HMCAD−FAD + 2-octynoyl-CoA interaction. This difference is presumably due lack of sensitivity of the stopped flow for measuring rate constants that are greater than 400 s^{-1}. Hence, we believe that the fast and slow relaxation rate constants for the reaction of HMCAD−FAD with all the C_8-CoAs employed herein are comparable with each other.

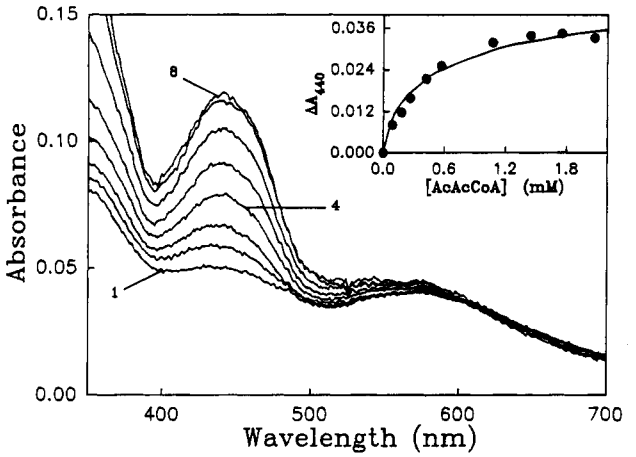

FIGURE 6: Effect of acetoacetyl-CoA on the spectral properties of the octanoyl-CoA-reduced enzyme charge-transfer complex. The latter was generated by mixing 10 μM HMCAD−FAD and 12 μM octanoyl-CoA. The concentrations of acetoacetyl-CoA for spectra 1−8 are 0, 0.092, 0.264, 0.574, 1.078, 1.75, 2.34, and 2.55 mM, respectively. Inset shows the increase in absorbance at 440 nm as a function of the total concentration of acetoacetyl-CoA. The solid line is the best fit of the experimental data for an equilibrium dissociation constant of 155 nM.

Dissociation Constants of 2-Octenoyl-CoA from MCAD−FAD(H_2) Sites. We and others have reported the 2-octenoyl-CoA-dependent changes in the spectral properties of pig kidney MCAD−FAD (Kumar & Srivastava, 1994; Lau et al., 1989). Figure 5A shows nearly identical spectral changes for the interaction of 2-octenoyl-CoA with human liver MCAD−FAD. Taking advantage of the maximal absorption changes at 442 nm, we proceeded to determine the dissociation constant of the enzyme−octenoyl-CoA complex. Figure 5B shows the titration result of a limiting concentration of HMCAD−FAD with increasing concentrations of 2-octenoyl-CoA. Note that as the concentration of 2-octenoyl-CoA increases, the net absorption change at 442 nm increases and then attains a plateau. The solid line is the best fit of the experimental data for a dissociation constant of 153 nM. It should be pointed out that this value is similar to the K_i (360 nM) for 2-octynoyl-CoA, determined from the data of Figure 1.

Recently, we demonstrated that in the presence of acetoacetyl-CoA, the reduced enzyme−octenoyl-CoA charge-transfer complex is converted into MCAD−FAD−acetoacetyl-CoA (Kumar & Srivastava, 1995). This process occurs via the reversal of the reductive half-reaction of the enzyme (eq 2).

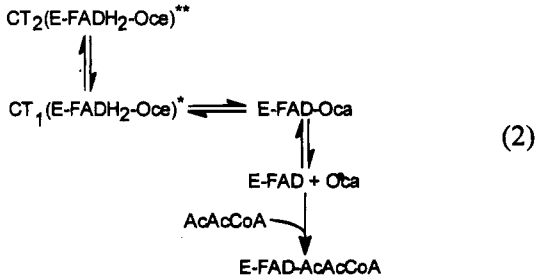

(2)

A qualitatively similar type of reversal of the reductive half-reaction of the enzyme in the presence of *S*-heptadecyl-CoA has been demonstrated by Thorpe et al. (1981).

Figure 6 shows the acetoacetyl-CoA-dependent spectral changes of the HMCAD−$FADH_2$−octenoyl-CoA charge-transfer complex. Note that as the concentration of acetoacetyl-CoA increases, the absorption at 440 nm (due to formation of the HMCAD−FAD−acetoacetyl-CoA) increases. A plot of ΔA_{440} as a function of total concentration of acetoacetyl-CoA is shown as the inset of Figure 6. The solid line is the best fit of the experimental data [according to Kumar and Srivastava (1995)] for an equilibrium constant (for the conversion of the charge-transfer complex to HMCAD−FAD) of 155 nM. It is noteworthy, once again, that this value is similar to the observed dissociation constant for the enzyme−octenoyl−CoA complex (153 nM) as well as the K_i for the enzyme−octynoyl-CoA complex (360 nM).

DISCUSSION

The purification protocol presented herein routinely yields 100−150 mg of highly purified HMCAD protein from 80 L of bacterial culture. The absence of any detectable contaminating protein bands on SDS−PAGE, the lack of any contaminating peaks during protein microsequencing, and the specific activity (utilizing IPCoA as substrate) of this enzyme all attest to the high degree of purity of the final preparation of HMCAD.

A comparative account of the kinetic properties of the pig kidney and human liver enzymes reveal that the K_m (for acyl-CoAs) and k_{cat} values for the dehydrogenase reaction are not substantially different among aliphatic acyl-CoA substrates of chain lengths C_4 to C_{10}. These parameters are also similar for the chromogenic substrate furylpropionyl-CoA (FPCoA). The K_m values for indolepropionyl-CoA (IPCoA) and [(4-dimethylamino)phenyl]propionyl-CoA (DPCoA) are also identical for these enzymes, but the k_{cat} values for the human liver enzyme utilizing these substrates are about 6−8-fold higher than those obtained for the pig kidney enzyme. Hence, it appears plausible that the substrates which undergo dehydrogenation reactions with optimal efficiencies (e.g., octanoyl-CoA, FPCoA etc.) exhibit identical kinetic properties with both human liver and pig kidney enzymes. On the other hand, the poor substrates (e.g., IPCoA and DPCoA) are dehydrogenated more efficiently with the human liver enzyme than with the pig kidney enzyme. We are currently in the process of extending these study to additional acyl-CoA substrates, and we will report these findings subsequently.

Another interesting aspect of the above comparative studies is the lower oxidase activity of the human liver enzyme than the pig kidney enzyme. With IPCoA as substrate, the k_{cat} for the oxidase reaction involving the human liver enzyme is about 5-fold slower than the pig kidney enzyme. We could not determine the K_m for IPCoA during the HMCAD-catalyzed oxidase reaction, since the reaction velocity appeared saturated even when the IPCoA concentration was as low as 0.1 μM. This was not unexpected in the light of our previous conclusion that the MCAD-catalyzed "dehydrogenase" and "oxidase" pathways branch following the formation of the Michaelis complex (Johnson et al., 1994; Srivastava et al., 1995). Since the k_{cat}/K_m ratio is a function of "free" rather than "bound" enzyme species, for a common substrate (e.g., IPCoA) and enzyme (e.g., HMCAD) this ratio must be the same for the two branching pathways, i.e., "dehydrogenase" and "oxidase" reactions (Srivastava et al., 1995).

Kinetic Mechanism of the 2-Octynoyl-CoA-Dependent Inactivation of HMCAD. Having satisfied the following two

criteria, we employed Tsou's method (1988) for deducing the kinetic mechanism of the 2-octynoyl-CoA-dependent inactivation of the enzyme. These criteria include the following: (1) The rate of inactivation of the enzyme must be considerably slower than the rate of catalysis. (2) The total concentration of the substrate and inactivator can be taken to be equal to their free concentrations. Of these, the first criterion was naturally satisfied since k_{cat} for HMCAD utilizing IPCoA as substrate (3.4 s^{-1}) was 60−140 fold higher than the k_{inact} (0.024−0.060 s^{-1}) of the enzyme. The second criterion was satisfied by experimental design. The concentrations of the substrate, inactivator and enzyme were selected such that the enzyme progress curves attained a plateau without substantial (<10%) consumption of the substrate. Hence, the total concentration of substrate was taken to be the measure of its free concentration during the entire course of the reaction. Since the concentration of the enzyme was 2−3 orders of magnitude lower than the concentration of the inactivator, a negligible fraction of the inactivator was consumed, and thus its total concentration served as a measure of its free concentration.

When the enzyme-catalyzed reaction progress curves of Figure 1A (which conformed to the above criteria) were examined in light of Tsou's theoretical model (1988), it became obvious that the 2-octynoyl-CoA-modified enzyme possessed no residual catalytic activity and that the inactivation of the enzyme was irreversible in nature. These predictions rely on the fact that all of the enzyme-catalyzed reaction progress curves attained horizontal (rather than increasing) asymptotes. Consistent with the above model, all of the reaction progress curves satisfying the above criteria conformed to the first-order rate law, and the observed rate constants showed hyperbolic dependence on the 2-octynoyl-CoA concentrations (Figure 1B). This pattern suggested that the 2-octynoyl-CoA-dependent inactivation proceeded via formation of the enzyme−octynoyl-CoA complex. Furthermore, the linear dependence of $K_{0.5}$ (the concentration of 2-octynoyl-CoA required to attain half of the total changes in the rate constants, Figure 1B) on the substrate concentrations (e.g., Figure 1C) attested to the fact that 2-octynoyl-CoA and IPCoA served as competitive ligands for binding at the enzyme site. A cumulative account of all these deductions lead to a minimal model (eq 3) for the enzyme-

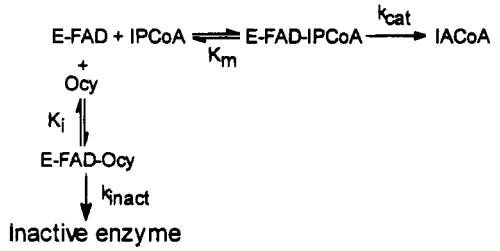

(3)

catalyzed reaction in the presence of 2-octynoyl-CoA. In eq 3, Ocy refers to 2-octynoyl-CoA. On the assumption that the binding steps satisfy the rapid-equilibrium conditions, the time-dependent appearance of IACoA for the model of eq 3 can be represented as follows:

$$[IACoA] = \frac{v^* [E\text{-}FAD]_t}{k_{obs}} (1 - e^{-k_{obs} * t}) \quad (4)$$

where

$$v^* = \frac{k_{cat} [IPCoA]/K_m}{1 + [IPCoA]/K_m + [Ocy]/K_i} \quad (5)$$

$$k_{obs} = \frac{k_{inact} [Ocy]}{K_i + K_i [IPCoA]/K_m + [Ocy]} \quad (6)$$

Equation 6 predicts a hyperbolic dependence of k_{obs} on 2-octynoyl-CoA concentration, as evident from the data of Figure 1B. The concentration of octynoyl-CoA required to attain half of the maximal saturation ($K_{0.5}$) can be given by eq 7.

$$K_{0.5} = K_i + K_i [IPCoA]/ K_m \quad (7)$$

According to eq 7, $K_{0.5}$ is linearly dependent upon concentration of IPCoA, as evident from the data of Figure 1C, with the magnitudes of intercept and slope being equal to K_i and K_i/K_m. For IPCoA, the K_m and K_i (for 2-octynoyl-CoA) values thus determined were found to be 5.20 μM and 360 nM. Note that the K_m for IPCoA determined from the data of Figure 1 is similar to that determined (for the dehydrogenase reaction) by the conventional steady-state kinetic method (8.7 μM; Table 2). Also, the K_i for 2-octynoyl-CoA is similar to the observed equilibrium constant for dissociation of 2-octenoyl-CoA from the (HMCAD−FAD−octenoyl-CoA)** complex (153 nM) as well as the equilibrium constant for the dissociation of the (HMCAD−$FADH_2$−octenoyl-CoA)** charge-transfer complex to HMCAD−FAD + octanoyl-CoA (155 nM; see below).

Comparative Microscopic Pathways for Interactions of Differently α,β-Unsaturated C_8-CoAs with HMCAD−FAD. The experimental results presented in the previous section suggest that the spectral changes of HMCAD−FAD are significantly different with different C_8-CoAs. Since octanoyl-CoA is a substrate of the enzyme, the octanoyl-CoA-dependent spectral changes are manifested in the reduction of the enzyme-bound flavin. In contrast, the 2-octenoyl-CoA- and 2-octynoyl-CoA-dependent spectral changes are due to perturbations in the electronic structure of the oxidized flavin. It should be pointed out that the fast spectral changes (Figure 2A inset and Figure 3) in the presence of 2-octynoyl-CoA are *not* due to the inactivation of the enzyme; the inactivation reaction accompanies 3−4 orders of magnitude slower spectral changes (Figure 2).

As observed with the pig kidney enzyme, the transient courses of the HMCAD−FAD + octanoyl-CoA (chemical transformation) and HMCAD−FAD + octenoyl-CoA (physical interaction) reactions are consistent with two observed relaxation phases. The magnitudes of the fast and slow relaxation rate constants are similar for these ligands. Since the fast and slow relaxation rate constants exhibit apparent zero-order dependence on individual ligand concentrations (within the range required to satisfy the pseudo-first-order conditions; Figure 4), it follows that the corresponding enzyme−ligand Michaelis complexes must be formed prior to the observed relaxation phases. A similar situation prevails for the interaction of HMCAD−FAD with 2-octynoyl-CoA (Figure 3). The latter interaction is also a biphasic process, with the magnitudes of the fast and slow relaxation rate constants being 2−3-fold higher than those observed with octanoyl-CoA and 2-octenoyl-CoA. Since the fast and slow relaxation rate constants in this case are also

apparently independent of the 2-octynoyl-CoA concentration (Figure 3), it follows that the enzyme−octynoyl-CoA Michaelis complex must be formed prior to the observed relaxation phases. These results suggest similarity in the microscopic pathways for the HMCAD−FAD + C_8-CoA interactions (eq 8).

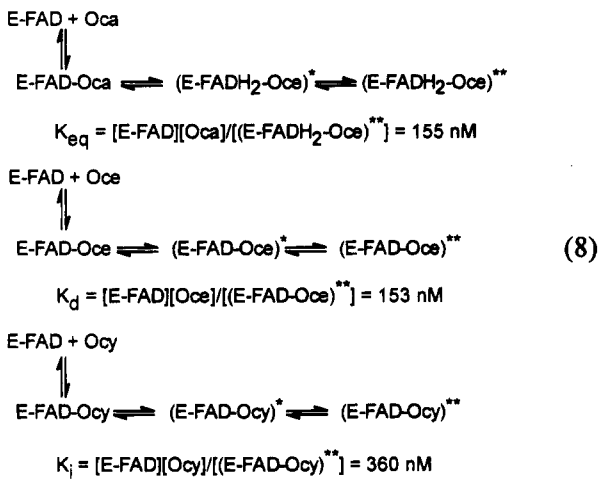

(8)

The above similarity is further attested by the fact that the equilibrium constants (for reversal of the overall reactions of eq 8) are nearly identical. In the case of octanoyl-CoA, the equilibrium constant (K_{eq} = 155 nM) is a measure of the reversal of the overall reductive half-reaction of the enzyme (Figure 6); with 2-octenoyl-CoA, it is a measure of the dissociation constant (K_d = 153 nM) of the stable form of the enzyme−octenoyl-CoA complex (Figure 5); and with 2-octynoyl-CoA, it is a measure of the inhibition constant (K_i = 360 nM) of the IPCoA-dependent dehydrogenase reaction of the enzyme (Figure 1). Clearly, the kinetic and thermodynamic parameters for the interactions of functionally diverse C_8-CoAs with HMCAD−FAD are remarkably similar.

Why are the kinetic and thermodynamic parameters for the interactions of functionally diverse C_8-CoAs with the enzyme so similar? This is particularly important since all these C_8-CoA ligands induce different types of spectral changes upon interactions with the enzyme. Although a definitive answer to this question must await further studies, it appears plausible that some common physical process is involved in dictating similar kinetic and thermodynamic patterns with these C_8-CoAs. We propose that this common process is an obligatory protein conformational change, and this process occurs during the observed relaxation phases following the formations the individual HMCAD−FAD−C_8-CoA complexes. In the case of octanoyl-CoA, the protein conformational change is coupled to the reductive half-reaction, whereas in the case of 2-octenoyl-CoA and 2-octynoyl-CoA, it is coupled to the changes in the electronic structures of both oxidized flavin and corresponding CoAs. This proposition is consistent with Bernhard's theory (1981) that the protein conformational changes are often coupled to changes in the (enzyme-bound) ligand structures.

In light of the above discussions, it is evident that the enzyme species which undergoes inactivation is (HMCAD−FAD−octynoyl-CoA)** [analogous to (HMCAD−$FADH_2$−octenoyl-CoA)** and (HMCAD−FAD−octenoyl-CoA)** complexes; see eq 8], whereas the enzyme species that undergoes the reductive half-reaction is HMCAD−FAD−octanoyl-CoA Michaelis complex. Hence, the microscopic step responsible for the 2-octynoyl-CoA-dependent inactivation of the enzyme is *entirely different* than that responsible for the octanoyl-CoA-dependent reductive half-reaction of the enzyme. Therefore, from the kinetic mechanism point of view, 2-octynoyl-CoA cannot be assigned as a *"mechanism-based"* inactivator of the enzyme (Powell & Thorpe, 1988). The inactivation of the enzyme by covalent modification of Glu-376 in the presence of 2-octynoyl-CoA is merely due to happenstance of the structural features of the enzyme−ligand complexes (see below).

Protein Structural Basis of the Octanoyl-CoA-Dependent Reductive Half-Reaction and the 2-Octynoyl-CoA-Dependent Inactivation of HMCAD. The question arises of whether the octanoyl-CoA-dependent reductive half-reaction and the 2-octynoyl-CoA-dependent inactivation of the enzyme occur during the same microscopic steps or not. In attempting to answer this question, we realized that both these reactions are, in part, limited by the rates of proton abstractions from the α (C2)- and γ (C4)-carbon atoms of their cognate C_8-CoAs (McFarland, 1991; Powell & Thorpe, 1988). Clearly, the abstraction of the C2-proton (in case of octanoyl-CoA) is 3−4 orders of magnitude more efficient than the C4-proton (in case of 2-octynoyl-CoA). Although the efficiency of proton transfer (in chemical reactions) is known to be dictated by several factors, e.g., difference in pK_as of donor and acceptor groups, resonance stabilization of resulting anions, solvation of ground state and activated complexes, hydrogen bonding, etc. (Jencks, 1987), we propose that in the present situation the structure of the enzyme plays a dominant role in modulating the efficiency of the proton transfer from C2 versus C4 of C_8-CoAs.

On the basis of the X-ray crystallographic structures of pig liver MCAD in the absence (referred herein as "apo") and presence ("holo") of C_8-CoA (Kim & Wu, 1988; Kim et al., 1993), it is evident that although the global protein structure remains unchanged, there are some noticeable changes in the local structure. Among these, the relocation of the carboxyl-group of Glu-376 (swinging away from C2 of C_8-CoA) is most noteworthy (Figure 7). The carboxyl oxygens of Glu-376 (viz., OE1 and OE2) move 1.1 and 3.78 Å from their positions in the "apo" structure upon formation of the "holo" structure. Considering that the protein conformational changes occur following the formations of the enzyme−C_8-CoA Michaelis complexes (which occur without substantial changes in the electronic structures of the individual components), we propose that the Michaelis and the stable forms of the isomerized complexes [e.g. (HMCAD−$FADH_2$−octenoyl-CoA)** and (HMCAD−FAD−octynoyl-CoA)** complexes; eq 8] are representative of the known "apo" and "holo" conformations of the enzyme, respectively.

Assuming that the binding mode of C_8-CoA remains the same in these protein structures, OE2 in the apo structure is 2.39 Å distance from C2 (Figure 7), an ideal situation for efficient proton transfer between these atoms (Komives, 1991). Such a situation does not prevail for the transfer of C2-proton when OE2 is in the holo conformation (distance between C2 and OE2(holo) = 4.65 Å). The distance between C4 and OE2 is neither favorable in apo (4.47 Å) nor in holo (4.83 Å) structure. These structural data suggest that the "price" of entropic loss (toward attaining the

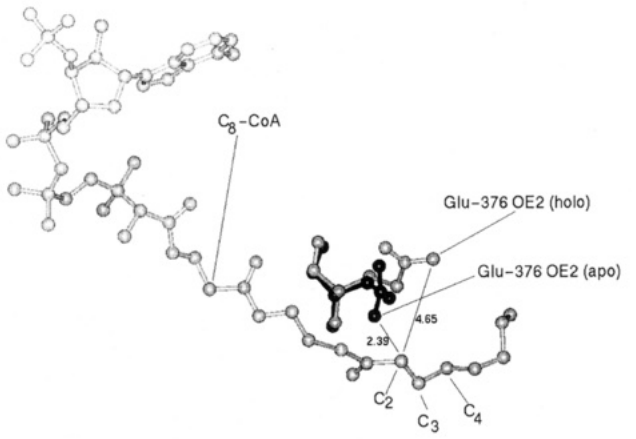

FIGURE 7: Alternative positions of Glu-376 within the X-ray crystallographic structures of pig liver MCAD in the absence ("apo", dark shade) and presence ("holo"; light shade) of C_8-CoA. The two oxygen atoms of Glu-376 carboxyl are represented by OE1 and OE2. The distances between OE2 (apo and holo) and C2 of C_8-CoA are shown. Other distances from OE1 and OE2 to C2, C3, and C4 carbon atoms (in Å) are as follows:

	C2	C3	C4
OE1(apo)	4.25	5.52	5.69
OE1(holo)	4.94	6.06	6.00
OE2(apo)	2.39	3.83	4.47
OE2(holo)	4.65	5.39	4.83

transition state) for the transfer of proton from C2 to OE2 is already paid in the form of maintaining an ideal ground-state structure between the proton donor (C2) and proton acceptor (OE2) atoms. In contrast, the direct transfer of proton from C4 to OE2 (the atom which is closest to C4 in both apo and holo structures) would require considerably higher structural rearrangements toward the attainment of the transition-state structure. Consequently, the proton transfer from C2 to OE2 is kinetically more favorable than that from C4 to OE2 and is responsible for the 3−4 orders of magnitude difference in the rate constants of the corresponding reactions.

ACKNOWLEDGMENT

We are thankful to Dr. J.-J. P. Kim for providing us the coordinates of pig liver MCAD before they were released from the Brookhaven Protein Data Bank.

REFERENCES

Andresen, B. S., Bross, P., Jensen, T. G., Winter, V., Knudsen, I., Kolvraa, S., Jensen, U. B., Bolund, L., Duraan, M, Kim, J.-J. P., Curtis, D., Divry, P., Saban, C. V., & Gregersen, N. (1993) *Am. J. Hum. Genet. 53*, 730−739.

Bernert, J. T., & Sprecher, H. (1977) *J. Biol. Chem. 252*, 6737−6744.

Bernhard, S. A. (1981) *Stud. Org. Chem. (Amsterdam) 10*, 237−252.

Brackett, J. C., Sims, H. F., Steiner, R. D., Nunge, M., Zimmerman, E. M., deMartinville, B., Rinaldo, P., Slaugh, R., & Strauss, A. W (1994) *J. Clin. Invest. 94*, 1477−1483.

Bradford, M. (1976) *Anal. Biochem. 72*, 248−254.

Bross, P., Engst, S., Strauss, A. W., Kelly, D. P., Rasched, I., & Ghisla, S. (1990) *J. Biol. Chem. 265*, 7116−7119.

Bross, P., Andresen, B. S., Winter, V., Krautle, F., Jensen, T. G., Nandy, A., Kolvraa, S., Ghisla, S., Bolund, L., & Gregersen, N. (1993) *Biochim. Biophys. Acta 1182*, 264−274.

Freund, K., Mizzer, J., Dick, W., & Thorpe, C. (1985) *Biochemistry 24*, 5996−6002.

Gregersen, N., Andersen, B. S., Bross, P., Winter, V., Rudiger, N., Engst, S., Christensen, E., Kelly, D., Strauss, A. W., Kolvraa, S., Bolund, L., & Ghisla, S. (1991) *Hum. Genet. 86*, 545−551.

Jencks, W. P. (1987) *Catalysis in Chemistry and Enzymology*, Dover Publications, Inc., New York.

Johnson, J. K., & Srivastava, D. K. (1991) *Arch. Biochem. Biophys. 287*, 250−256.

Johnson, J. K., & Srivastava, D. K. (1993) *Biochemistry 32*, 8004−8013.

Johnson, J. K., Wang, Z. X., & Srivastava, D. K. (1992) *Biochemistry 31*, 10564−10575.

Johnson, J. K., Kumar, N. R., & Srivastava, D, K. (1993) *Biochemistry 32*, 11575−11585.

Johnson, J. K., Kumar, N. R., & Srivastava, D. K. (1994) *Biochemistry 33*, 4738−4744.

Kelly, D. P., Kim, J.-J. P., Billadello, J. J., Hainlin, B. E., Chu, T. W., & Strauss, A. W. (1987) *Proc. Natl. Acad. Sci. U.S.A. 84*, 4068−4072.

Kelly, D. P., Whelan, A. G., Ogden, M. L., Alpers, R., Zhang, G., Bellus, G., Gregersen, N., Dorland, L., & Strauss, A. W. (1990) *Proc. Natl. Acad. Sci. U.S.A. 87*, 9236−9240.

Kim, J.-J. P., & Wu, J. (1988) *Proc. Natl. Acad. Sci. U.S.A. 85*, 6677−6681.

Kim, J.-J. P., Wang, M., & Paschke, R. (1993) *Proc. Natl. Acad. Sci. U.S.A. 90*, 7523−7527.

Komives, E. A., Chang, L. C., Lolis, E., Tilton, R. F., Petsko, G. A., & Knowles, J. R. (1991) *Biochemistry 30*, 3011−3019.

Kumar, N. R., & Srivastava, D. K. (1994) *Biochemistry 33*, 8833−8841.

Kumar, N. R., & Srivastava, D. K. (1995) *Biochemistry 34*, 9434−9443.

Lau, S.-M., Brantley, R. K., & Thorpe, C. (1989) *Biochemistry 28*, 8255−8262.

Lehman, T. C., Hale, D. E., Bhala, A., & Thorpe, C. (1990) *Anal. Biochem. 186*, 280−284.

Matsubara, Y., Narisawa, K., Miyabayashi, S., Tada, K., Coates, P. M., Bachmann, C., Elsa, L. J., Pollitt, R. J., Rhead, W. J., & Coates, C. R. (1990) *Biochem. Biophys. Res. Commun. 171*, 498−505.

McFarland, J. T. (1991) *Enzyme Mechanism from Isotope Effects* (Cook, P. F., Ed.) pp 151−179, CRC Press, Inc., Boca Raton, FL.

McFarland, J. T., Lee M., Reinsch, J., & Raven, W. (1982) *Biochemistry 21*, 1224−1229.

Powell, P. J., & Thorpe, C. (1988) *Biochemistry 27*, 8022−8028.

Roe, C. R., & Coates, P. M. (1989) in *The Metabolic Basis of Inherited Disease* (Scriver, C. R., Beauder, A. L., Sly, W. S., & Valle, D., Eds.) pp 889−914, McGraw-Hill, New York.

Saijo, T., Welch, W. J., & Tanaka, K. (1994) *J. Biol. Chem. 269*, 4401−4408.

Sambrook, J., Fritsch, E., & Maniatis, T. (1989) in *Molecular cloning: A Laboratory Manual*, 2nd ed., Cold Spring Harbor Laboratory, Cold Spring Harbor, New York.

Schulz, A. R. (1994) in *Enzyme Kinetics: From Diastase to Multi-Enzyme Systems*, Cambridge Univesity Press, New York.

Srivastava, D. K., Kumar, N. R., & Peterson, K. L. (1995) *Biochemistry 34*, 4625−4632.

Studier, F., Rosenberg, A., Dunn, J., & Dubendorff, J. (1990) *Methods Enzymol. 185*, 60−89.

Thorpe, C., Matthews, R. G., & Williams, C. H., Jr. (1979) *Biochemistry 18*, 331−337.

Thorpe, C., Ciardelli, T. L., Stewart, C. J., & Wieland, T. (1981) *Eur. J. Biochem. 118*, 279−282.

Tsou, C. L. (1988) *Adv. Enzymol. Relat. Areas Mol. Biol. 61*, 381−436.

Weber, K., & Osborn, M. (1969) *J. Biol. Chem. 244*, 4406−4412.

Yokota, I., Indo, Y., Coates, P. M., & Tanaka, K. (1990) *J. Clin. Invest. 86*, 1000−1003.

Yokota, I., Saijo, T., Vockley, J., & Tanaka, K. (1992) *J. Biol. Chem. 267*, 26004−26010.

Zahler, W. L., Barden, R. E., & Cleland, W. W. (1968) *Biochim. Biophys. Acta 164*, 1−11.

BI950898I